



NIH Public Access

Author Manuscript

Anal Chem. Author manuscript; available in PMC 2014 September 17.

Published in final edited form as:

Anal Chem. 2013 September 17; 85(18): . doi:10.1021/ac401830m.

Time-of-Flight Secondary Ion Mass Spectrometry based Molecular Histology of Human Spinal Cord Tissue and Motor Neurons

Jörg Hanrieder^{§,Φ}, Per Malmberg^{§,‡}, Olle R. Lindberg[#], John S. Fletcher[‡], and Andrew G. Ewing^{§,Φ,‡,*}

[§]National Center for Imaging Mass Spectrometry, Gothenburg University and Chalmers University of Technology, Sweden

^ΦDepartment of Chemical and Biological Engineering, Analytical Chemistry, Chalmers University of Technology, Gothenburg Sweden

[‡]Department of Chemistry and Molecular Biology, Analytical Chemistry, Gothenburg University, Gothenburg, Sweden

[#]Center for Brain Repair and Rehabilitation, Institute of Neuroscience and Physiology, Sahlgrenska Academy, University of Gothenburg, Gothenburg, Sweden

Abstract

Secondary ion mass spectrometry is a powerful method for imaging biological samples with high spatial resolution. Whole section ToF SIMS scans and multivariate data analysis have been performed on human spinal cord in order to delineate anatomical regions of interest based on their chemical distribution pattern. ToF SIMS analysis of thoracic spinal cord sections was performed at 5µm resolution within 2 hours. Multivariate image analysis by means of principal component analysis and maximum auto correlation factor analysis resulted in detection of more than 400 m/z peaks that were found to be significantly changed. Here, the results show characteristic biochemical distributions that are well in line with major histological regions, including grey and white matter. As an approach for iterative segmentation, we further evaluated previously outlined regions of interest as identified by multivariate image analysis. Here, further discrimination of the grey matter into ventral, lateral and dorsal neuroanatomical regions was observed. TOF SIMS imaging has been carried out at submicron resolution obtaining localization and characterization of spinal motor neurons based on their chemical fingerprint, including neurotransmitter precursors that serve as molecular indicators for motor neuron integrity. Thus, TOF SIMS can be used as an approach for chemical histology and pathology. SIMS holds immense potential for investigating the subcellular mechanisms underlying spinal cord related diseases including chronic pain and amyotrophic lateral sclerosis.

*Corresponding Author. Prof Andrew G. Ewing, University of Gothenburg, Analytical Chemistry, Kemivägen 10, SE-41296 Gothenburg, Sweden, andrew.ewing@chalmers.se, Phone: (+46) 31 7869113.

ASSOCIATED CONTENT

Supporting Information.

PCA and MAF Loading plots for all multivariate analyses

Single ion images

Co-localization images demonstrating origin of choline signals

Figure 1,3,4,5 in different color coding scheme

This material is available free of charge via the Internet at <http://pubs.acs.org>.

The authors declare no conflict of interest.

Keywords

TOF SIMS; Imaging Mass Spectrometry; Spinal Cord; Motor Neurons

INTRODUCTION

The spinal cord constitutes the interface of the peripheral and the central nervous system comprising essential circuits in motor control as well as somatosensory function. Anatomically, the tissue is generally separated into the white matter and grey matter. The white matter comprises the ascending and descending fiber tracts and surrounds the grey matter, which is composed of cell bodies. Primary somatosensory neurons from the dorsal root ganglion project to the dorsal horn dorsal horn of the grey matter. Here, somatosensory signaling between the peripheral and the central nervous system is relayed. In contrast spinal cord motor neurons are situated in the ventral grey matter and are essential for muscle control. The devastating, fatal neurodegenerative disease, amyotrophic lateral sclerosis (ALS), for instance is characterized by selective degeneration of spinal motor neurons.¹ Conversely, abnormal signaling events in the dorsal horn underlie development of chronic pain of neuropathic or inflammatory origin. However, the underlying pathomechanisms of ALS or chronic pain are still not understood. Complex biological and pathological processes involve the translocation of a wide range of chemical species. Chemical probing of the spatio-temporal dynamics of ongoing biochemical processes is therefore essential in order to deepen our understanding of complex biological mechanisms. A major objective when studying molecular mechanisms and interactions at the subcellular level is therefore the acquisition of molecular images for receiving spatial and temporal information of molecular abundance distribution. The main challenge in molecular imaging is to achieve appropriate temporal and spatial resolution with high precision, specificity, and sensitivity.

Imaging mass spectrometry (IMS) is an emerging technique for probing the molecular architecture of biological tissue in an anatomical context.² In contrast to common molecular biology techniques, IMS does not require any a priori knowledge of the potential target species. The technology allows the direct and comprehensive identification and spatial profiling of biomolecular species *in situ*, while maintaining high molecular specificity. Several IMS methods have been prevalent in biological studies including matrix assisted laser desorption/ ionization based imaging MS (MALDI IMS) and time-of-flight secondary ion mass spectrometry (ToF-SIMS) as well as several other related methods.³ MALDI IMS has been demonstrated to be a valuable approach in biomedical research although the technique currently has limitations with respect to lateral resolution and detection of low molecular weight compounds (<700Da) due to interference of matrix cluster ions.^{3,4} Mass range limitations in MALDI have been overcome by elegant approaches using e.g. isotopically labeled matrix or targeted MS/MS based analyte detection and quantification.^{5,6} Advances in ion source design have been presented to overcome limitations in spatial resolution by using highly focused beams (microprobe)⁷, oversampling⁸ or transmission geometry MALDI.⁹ While these developments represent important advances in the field of high-resolution laser desorption ionization based imaging mass spectrometry, limitations remain with respect to acquisition time, reproducibility and sensitivity when the spatial resolution and mass limits are extended. An integral advantage of SIMS based imaging MS is the possibility to acquire high-resolution images without compromising sample treatment procedures.

To date, the application of SIMS has been limited due to its restricted molecular mass range owing to the inability of conventional atomic ion beams to eject larger molecular species. This has been overcome by the development of cluster-ion beams, mainly Bi₃^{10,11} and

C_{60}^{12} , facilitating SIMS application for analysis of intact biomolecular species, including metabolites, lipids and small neuropeptides. SIMS imaging features high spatial resolution, often at the subcellular scale (<500 nm), which is unprecedented despite recent advances in other imaging mass spectrometry techniques. These features make SIMS a powerful technology for spatially profiling lipids and metabolites at the single cell level.¹³ This is of particular relevance for studying complex and heterogeneous samples, such as neuronal tissue and cells, which arguably constitute the most complex and least understood systems in the human body.¹⁴ The technique represents therefore a promising approach for investigating spinal cord biochemistry. Multiple IMS based studies on spinal cord have been reported previously providing important data on spinal cord pathology.^{15–21} In the present study, we probed the native distribution of lipids and metabolites in human spinal cord using ToF-SIMS for high spatial resolution imaging. ToFSIMS imaging in conjunction with multivariate statistical analysis (MVA) tools was used for molecular histology-based dissection of anatomical features. We used this approach to identify anatomical regions of interest in human spinal cord as well as to identify single motor neurons, and to study neuronal lipid chemistry and metabolism *in situ*. The method offers a promising alternative to classical histological techniques, since it provides more complex biochemical information while maintaining spatial information.

EXPERIMENTAL SECTION

Chemicals and Reagents

All chemicals were of pro-analysis grade and purchased from Sigma Aldrich (St. Louis, USA). TissueTek - optimial cutting temperature compound (OCT) was purchased from Sakura Finetek (AJ Alphen aan den Rijn, The Netherlands). Water was purified with a Milli-Q (Millipore, Bedford, MA, USA) purification system.

Clinical Samples

Post-mortem spinal cord tissue samples of thoracic level from two human subjects were used in the study. The cause of death in the subjects was cardiac failure and myocardial infarction. At autopsy, the spinal cords were dissected, removed from the dura mater, and cut into 5-mm sections. The tissue was then immediately frozen on a metal plate maintained in liquid nitrogen and stored at –72 °C. Autopsy was performed with written approval from the family in accordance with Swedish rules and regulations at the time of autopsy.

Sample Preparation

Thoracic spinal cord sections (12 µm) were cut using a cryostate microtome (Thermo Scientific, Waltham, MA). Here the tissue chunk was mounted with optimum cutting temperature compound (OCT). Sections were cut and thaw-mounted on conductive glass slides (indium tin oxide, ITO, Bruker Daltonics, Bremen, Germany). The thaw mounted sections were dried under vacuum for 10 min and stored at –80 °C until further use. For SIMS experiments, 2 consecutive sections from each subject were analyzed.

ToF-SIMS Analysis

An ION-TOF V TOF-SIMS instrument (IONTOF GmbH, Münster, Germany) equipped with a Bi_3^+ cluster ion gun as primary ion source was used. For whole section analysis, data were acquired in high current bunched mode (HBC)²² with a primary ion current of 0.25 pA at 25 keV and a maximum ion dose was $1.5 \cdot 10^9 /cm^2$. Scans were acquired using the stage “scan macro raster function” with 10 shots per pixel on 0.4×0.4 mm areas with 200 measurements per mm resulting in a pixel resolution of 5 µm. This acquisition mode comprises stepwise acquisition of 0.4×0.4 mm patches. Here, each patch is acquired in

electrostatic raster mode where the beam is moved over the field of view. The whole tissue area is analyzed by stepwise acquisition of these patches as achieved by stepwise movement of the sample stage. Both positive and negative ion mode data were collected. High resolution images of ventral horn regions were collected in burst-alignment mode²² with a primary ion current of 0.04 pA at 25 keV and an ion dose of $8.8 \cdot 10^{11}/\text{cm}^2$. Here, 50 scans were acquired from a predefined quadratic scan area with 200 μm in edge length. Images comprising 512×512 pixels were acquired resulting in a spatial resolution 390 nm. The mass resolution in high current bunch mode was about $M/\Delta M = 5 \times 10^3$. Conversely, burst-alignment mode mass resolution was $M/\Delta M = 350$ FWHM at m/z 500. Therefore m/z values are specified with two digits in bunch mode and given as absolute values for burst aligned experiments.

Data Analysis

All spectra were acquired and processed with the Surface Lab software (v. 6.3 ION-TOF). All spectra were calibrated internally to signals of $[\text{C}]^+$, $[\text{CH}]^+$, $[\text{CH}_2]^+$, $[\text{CH}_3]^+$, $[\text{C}_5\text{H}_{15}\text{PNO}_4]^+$ and $[\text{C}_{27}\text{H}_{45}]^+$ were used as calibration points in positive mode and $[\text{C}]^-$, $[\text{CH}]^-$, $[\text{C}_2]^-$, $[\text{C}_3]^-$, $[\text{C}_{16}\text{H}_{31}\text{O}_2]^-$ and $[\text{C}_{18}\text{H}_{35}\text{O}_2]^-$ in negative ion mode. Two mass interval lists were created (one for each ion polarity) which contained the list of m/z values to be included in the multivariate analysis. Mass interval lists were created by peak search of all individual samples according to the following search parameters: $S/N > 3$, width 0.8 Da. The assigned mass peaks were collected in the same mass interval list and redundant peak assignments removed. Image data was exported into the *.bif6 format and loaded into PLS-Toolbox (v. 7.02, Eigenvector Research Inc., Wenatchee, WA) running under MatLab (v. 2012a, The MathWorks Inc., Natick, MA). Here data were subjected to principal components analysis (PCA) and maximum autocorrelation factor analysis (MAF). For PCA, data were pre-treated by means of mean centering and Poisson scaling. For bottom up statistics, peak area values were evaluated in Excel (v. 2010) using the “Statistical Analysis of Microarray data” (SAM) tool for grouped unpaired statistical analysis (t-statistics).²³ The SAM tool was originally developed for microarray analysis and allowed comprehensive and unbiased analysis of significant changes in abundance levels between two groups. Further analysis of single lipid peaks and comparisons between groups was performed with non-parametric ANOVA (Kruskal Wallis) followed by *post hoc* analysis (Tukey HSD test) with 95% confidence interval.

Immunohistochemistry

After ToF SIMS analysis, spinal cord sections were fixed in 4% phosphate-buffered (0.1 M, pH 7.4) 4% paraformaldehyde (PFA) for 30 min. The sections were then washed in Tris-buffered saline (TBS) followed by blocking in TBS with 3% donkey serum and 0.2% Triton-X, prior to primary antibody incubation at 4°C, overnight (monoclonal mouse anti α-NeuN, 1:100, clone A60, Millipore). After additional washing with TBS, the sections were incubated with secondary antibody (biotinylated donkey α-mouse, Jackson ImmunoResearch Laboratories, USA) for 1 h at room temperature. The sections were washed with TBS, followed by amplification with avidin–biotin complex (Vectastain ABC Elite, Vector Laboratories, USA) and then visualized with 3,3'-diamino benzidine (DAB, 0.25 mg/mL, Saveen Biotech, Limhamn, Sweden, 0.04% NiCl, 0.0001% H₂O₂). Sections were mounted on glass slides and coverslipped using NeoClear® (Merck, Darmstadt, Germany) and NeoMount® (Merck). Images were collected on a Leica DM6000 B microscope equipped with an Optronics Microfire camera (Optronics International).

RESULTS AND DISCUSSION

ToF-SIMS can be used to identify histological regions of interest in human spinal cord

In the present study, we report a ToF-SIMS imaging based molecular histology approach for MS data dependent segmentation of biological tissue into anatomical regions of interest based on their chemical profile. This approach was utilized to investigate the spatial distribution of lipid species in post mortem human spinal cord. The molecular mechanisms underlying spinal cord pathologies, including ALS and chronic pain are still not fully understood. To elucidate the chemical architecture of human spinal cord is therefore of central relevance. The initial step of this approach was the acquisition of whole scan image data. Here, subsets of two consecutive tissue sections per individual were analyzed in positive and negative ion-mode. The data were calibrated internally and reconstructed with a common mass interval list (binning) for both ion-modes. This resulted in a total number of eight imaging datasets, each at least 3 GB in size.

Imaging data from the eight datasets were subjected to unsupervised multivariate statistical image analysis by means of PCA and MAF. While multivariate analysis has become more and more relevant in biological SIMS imaging, only a few previous studies addressed the topic by comparing the performance of these approaches.^{24,25} Here, we aim to compare the performance of the two MVA tools with respect to contrast and their ability to identify anatomically relevant regions of interest. A further aim has been to exploit the potential of multivariate statistical methods to chemically identify and characterize individual nerve cells based on the corresponding intensity distribution of metabolites and lipids. The molecular species that outline the histological regions and cellular environments can then provide a further insight in local lipid biochemistry and metabolism.

Indeed using a top-down image analysis approach, the characteristic outline of the grey and white matter, respectively, has been observed in the second principal component and the third MAF factor, respectively (Fig. 1A). From the eigenvectors (loadings) of the corresponding PC or MA factor, the variables, i.e. m/z values, can be obtained that contribute most to the respective eigenvalues (i.e. PC- or MAF score) (Fig. 1B, SI Fig. 1,2). The calculated data for positive and negative mode show characteristic localization of various lipid species. Here phosphatidylcholine (PC) headgroup and intact phospholipids were detected in positive mode localized to the grey matter. In negative mode, fatty acids (FA) and phosphoinositols (PI) were found to be increased in the gray matter region (Fig. 2A, SI Fig.2). In contrast, localization of cholesterol derivatives, vitamin E and sphingomyelins (SM) to the white matter region were observed (Fig.2A), all detected in positive mode. In negative mode, predominantly cholesterol species (m/z 385.36, $[M-H]^-$) and vitamin E (m/z 430.29, $C_{29}H_{49}O_2$, $[M-H]^-$) were found increased in the white matter.

As an alternative approach for statistical analysis of imaging MS data, we have employed a previously reported bottom up strategy based on data extracted from outlined anatomical regions of interest data²⁶. Here, histological regions of interest have been assigned and data extracted by reconstructing the respective ROI's in the Surface Lab software (IonTof). The sum spectra of these ROI's are either total ion current (TIC) normalized or subjected to log₂ conversion and median normalization. The resulting data of all grey matter (GM) and white matter (WM) regions have been evaluated by means of multivariate, paired SAM analysis.²³ The results of the log₂/median normalized data show significant intensity changes ($p < 0.05$) for 336 m/z values in positive ion mode and 470 in negative ion mode, respectively that were found to be either increased or decreased in the grey matter compared to the white matter (Fig. 3A). Here, the most prominent signals were annotated based on accurate mass matching and comparison to values reported in the literature.²⁷ Among these findings, PC phospholipids were found to be the most prominent compounds, and these are elevated in

the grey matter (Fig. 2A, SI Fig.2). Similarly, cholesterol species are found relatively increased in the white matter (Fig.2B, Fig.3B, SI Fig.2). The results are well in line with the data obtained by top-down multivariate analysis as well as all previously reported data on SIMS imaging of nervous tissue.^{28,29} These findings highlight the potential of this unbiased segmentation approach for elucidating the chemical architecture of complex biological samples.

Iterative segmentation of predefined regions of interest to identify anatomical heterogeneities

To further investigate the potential of this approach, we have extracted IMS data of the grey matter ROI and submitted them to our two-step multivariate statistical analysis (MVA) workflow. Following initial dissection of spinal cord into two major regions of interest, grey matter and white matter, the goal was to further delineate these histological regions into sub-regions. The grey matter, as an example of previously outlined ROI's has been reconstructed for all samples with a common mass interval list in both positive and negative mode.

Similarly to the whole scan data, the ROI data have been subjected to PCA and MAF analysis. The results show that major variations detected with the multivariate tools originate from inaccuracies in region outlining as well as tissue damage. However, beyond these interferences the data analysis reveals characteristic sub-regions such as the ventral and dorsal horn of the spinal cord grey matter (Fig. 4A). In addition, the dorsal horn can be further segmented into its sub layers including the substantia gelatinosa of Rolando (SGR) and the adjacent dorsolateral fasciculus. These were only observed with MAF and not PCA. The chemical differences in between these regions have been deduced from the respective MAF loadings of the corresponding MAF-factor that outlines these sub-regions (Fig. 4B). Here, inspection of the respective MAF loadings and subsequent SAM analysis shows a number of compounds that are found to be significantly increased in the dorsal horn (Fig. 4C). Conversely, a number of compounds are identified that localize to the ventral and intermediate part of the ventral horn (Fig. 4D). Bottom up statistical analysis, by means of paired t-test using SAM, shows relative elevation of many compounds previously observed in MAF image analysis. Mandatory inspection of single ion images shows that the molecular species deduced from MVA results do indeed localize to the dorsolateral fasciculus (Fig. 4C), the substantia gelatinosa of Rolando, the lateral horn (LH), and the ventral horn (Fig. 4D).

The chemical species that show characteristically increased peak intensities in the dorsolateral fasciculus (DLF) include at least four different species (m/z 71.97 [Na_2CN]⁺, m/z 80.94 [Na_2Cl]⁺, m/z 87.95 [Na_2CNO]⁺ and m/z 164.92 [Na_2SO_4]⁺) (Fig. 4C). Interestingly, these compounds all comprise physiological salts, which have been identified based on their accurate mass as well as their predicted isotopic pattern. SIMS is particularly sensitive to salt ions that might in turn significantly affect ionization of other analytes.³⁰ The observed inorganic signals (Na_2Cl , Na_2SO_4) can be a result of atmospheric contaminations and reactions during the desorption process. However, Na^+ and Cl^- ions are of significant relevance in neuronal signaling. This for instance includes Na^+/Cl^- dependent neurotransmitter transporters, such as the dopamine transporter (DAT),³¹ which warrants the fact that these signals can be of endogenous origin. In addition, ToF SIMS based detection of organic salt signals (Na_2CN) as protein markers in human stem cells has been described previously, further supporting the fact that these salts are related to endogenous protein species.³² The dorsolateral fasciculus comprises unmyelinated fibers that terminate in the adjacent nerve roots (dorsal horn, Rexed lamina I). Elevated amounts of physiological salts could point to a different salt homeostasis in this anatomical region. In contrast, masses that are found elevated in the adjacent grey matter regions of the spinal cord include m/z 107.08 (hydroxyltropylium ion, $[\text{CH}_2\text{C}_6\text{H}_4\text{OH}]^+$) m/z 129.05 [$\text{C}_9\text{H}_7\text{N}$]⁺, m/z 369.33 ($\text{C}_{27}\text{H}_{45}$, [M]

$+H-H_2O]^+$), m/z 430.34 (vitamin E, C₂₉H₅₀O₂, [M+H]⁺), as well as an unknown peak at m/z 247.22 (Fig.4D). Here the mass peaks m/z 107.08 and m/z 129.05 were found particularly pronounced in the horseshoe shaped substantia gelatinosa of Rolando (SGR, Rexed laminae II) of the dorsal horn but showed also distributions located in the lateral horn and the ventral horn (Fig. 4D, arrow). Cholesterol and vitamin E showed a rather even distribution throughout the dorsal and ventral horn. These are typically associated with myelin sheaths of axon fibers, comprising the white matter. Increased amounts of white matter constituents points therefore to an extended degree of innervation by ascending and descending fiber tracks. The hydroxytropylumion (m/z 107.08, [CH₂-C₆H₄-OH]⁺) can originate from tyrosine (Tyr). Similarly m/z 129.05 corresponds to [C₉H₇N]⁺ another characteristic amino acid fragment originating from tryptophan. Both tyrosine and tryptophan are precursors for essential neurotransmitters (tyrosine: dopamine, norepinephrine, epinephrine and tryptophan: serotonin). Serotonergic projections typically terminate partly in the SGR of the dorsal horn and comprise major circuits in distal pain signaling. The distinct localization of serotonin to the SGR in the dorsal horn as well as more general distribution in the lateral and ventral horn has been described recently.³³ Similarly, descending adrenergic projections terminate in the intermediolateral nucleus of the lateral horn³⁴ as well as the Onuf's nucleus in the ventral horn.³⁵ Thus, the relevance of SIMS imaging is clear in mapping anatomical regions of neuroendocrine tissue based on its neurochemical profile, particularly when MAF statistics are used.

The results show that top-down image analysis by means of MAF statistics is a powerful approach to delineate histological features on a molecular basis. In contrast to PCA, MAF employs an implemented correction to the noise covariance matrix. This is achieved by an iterative comparison to adjacent pixel spectra. This approach is therefore not dependent on data preprocessing (e.g. scaling, Poisson correction) and thus provides a better contrast, more sensitive image that can be used to catch slight intra tissue heterogeneities. Although, similar observations have been reported before,^{24,25} these variations in performance are hard to quantify in an unbiased way. For instance, PCA proves to be advantageous for detection of more general features, while MAF captures slight heterogeneities such as tissue damage resulting in background signal originating from the underlying surface. In this context it has been previously demonstrated that PCA can perform similarly to MAF depending on the sample as well as data pre-treatment (scaling, centering).²⁵ MAF data inspection is, however, more time consuming since the technique is more computationally demanding. This might be a relevant disadvantage for analysis of multiple large datasets. However, given its robustness in performance and independence of data pre-treatment procedures, MAF is favorable for image analysis on the smaller scale.

Imaging single nerve cells *in situ*

Experiments have been carried out to investigate the potential of ToF-SIMS in conjunction with top down MVA for probing the biochemistry of single nerve cells. In order to delineate lipid architecture on a subcellular scale, we have used burst aligned mode experiments on ventral spinal cord regions. The acquired imaging data have been evaluated using top down multivariate statistical analysis by means of PCA and MAF (Fig. 5, SI Fig. 3,4). Here, we observe multiple cell body like features that are detected in different principle component- and MAF factor-composition images (Fig. 5A,B) in both positive (Fig. 5 A,B I-II) and negative mode (Fig. 5A,B III-IV). Although the first PC and MAF factors mainly have been used to identify tissue heterogeneities (i.e. grey matter and white matter), cell like features are identified in successive components (Fig. 5A,B). To further evaluate the performance of PCA and MAF, we have compared how the respective loadings represent true chemical localizations (Fig. 5C,D). The data show that the major loadings as identified with MAF, are indeed chemical species that are increased or decreased in the nerve cell regions. In order to

validate the identity of the observed cell-like features, immunohistochemistry staining with neuron specific antigen NeuN³⁶ has been performed and this confirmed that the observed features are indeed nerve cells (Fig. 5D III, 5D IV). Cell size and morphology suggest that these cells are alpha motor neurons. These data again demonstrate the better performance of MAF compared to PCA for analyses of this type.

Inspection of the PCA and MAF loadings allows deduction of what molecular species are significantly localized to the nerve cells (SI Fig. 3,4). Here the eigenvectors (loadings) of the variables (*m/z*) for the respective PCA and MAF scores/factors can be identified, thus outlining nerve cells from background tissue. The data reveal that choline (*m/z* 104) and its major fragment triethylenimine (*m/z* 86, [C₅H₁₂N]⁺) are characteristically increased in motor neurons (Fig. 5C I-II) as revealed by MAF in MAF-factor 2 in the positive ion mode. In order to verify that these choline signals do not originate from intact phosphatidylcholine (PC) headgroup (*m/z* 184, [C₅H₁₅PO₄N]⁺), ion images of *m/z* 184 and a major PC headgroup fragment *m/z* 166 [C₅H₁₃PO₃N]⁺ have been generated (Fig. 5D1-II). While some of the choline and triethylenimine signal indeed originates from PC, no co-localization to distinct sub-cellular features was observed (Fig. 5CI-II, 5DI-II). Triethylenimine can furthermore originate from amino acids, since it represents the immonium ion of leucine/isoleucine (Leu/Ile) as well as a characteristic fragment of lysine (Lys). Therefore, single ion images of other characteristic leucine/isoleucine and lysine fragments have been inspected, including, *m/z* 30 ([CH₄N]⁺, general amino acid fragment), *m/z* 70 ([C₄H₈N]⁺, Leu/Ile fragment), *m/z* 84 ([C₅H₁₀N]⁺, Lys fragment) (SI Fig.5 I-VI). In addition, other major fragments of common amino acids arginine, phenylalanine and tyrosine (Arg, Phe, Tyr) show no distinct localization to the nerve cells (SI Fig.5 VII-IX). All in all, this suggests that the observed choline signals are not an artifact of intact phospholipids, or amino acids, and represent free choline.

Detection of free choline is of great relevance, since choline serves as precursor for the neurotransmitter acetylcholine. The presynaptic hemicholinium-3, sensitive high affinity choline transporter (CHT) has been identified previously to be specifically overexpressed in motor neurons.³⁷ Elevated choline levels can therefore serve as chemical markers for probing motor neurons integrity and activity using IMS. However, to date, label free subcellular detection of choline *in situ* or *in vivo* has not been possible. Since choline is not electroactive, direct electrochemical detection, as typically used for neurochemicals *in vivo* is also not possible, requiring application of enzyme-coated electrodes. These in turn suffer from limitations in terms of sensitivity, sampling rate, and specificity. Other methods involve perturbation of the sample using different staining protocols. Choline is typically monitored using chemical shift imaging. However this method is limited in terms of spatial resolution. Therefore, ToF SIMS-based choline imaging in individual nerve cells represents an important advance for characterizing neurochemical processes at the single cell level.

In addition to choline signals, cholesterol (*m/z* 369, [M+H-H₂O]⁺) was found to be decreased in the corresponding MAF factor (MAF2). Cholesterol is a major component of myelin that surrounds neuronal processes, i.e. axons, and is primarily found in the white matter. Although these processes innervate the grey matter to some extent, they are not localized to the actual cell bodies that constitute the majority of the grey matter. Furthermore, several unknown compounds with *m/z* 93 and *m/z* 137, have been found here to co-localize with the nerve cells in negative mode (Fig. 5C III-IV). Although it has not been possible to identify to date these compounds *in situ*, this provides further potential targets for subcellular imaging.

CONCLUSIONS

The present study demonstrates the potential of ToF-SIMS imaging for interrogating the biochemical architecture of human neural tissue and cells. Multivariate statistics have been used for exploratory analysis of SIMS imaging data using complementary top down and bottom up strategies. These provide a robust and powerful approach to obtain chemical information for histological regions of interest. In these applications, MAF is found to be superior to PCA-based image analysis. Finally, submicron imaging of individual nerve cells *in situ* followed by multivariate statistics has been used for characterization of intact motor neurons based on their endogenous neurochemical profiles. In these experiments we demonstrate detection of free choline localized to the white matter. These data suggest an approach for future investigations concerning motor neuron degeneration, since it can be used to reveal disturbances in the neurochemical interplay affecting neuronal functionality and integrity.

Supplementary Material

Refer to Web version on PubMed Central for supplementary material.

Acknowledgments

This work was supported by the European Research Council (AGE ERC advanced grant), the Wallenberg Foundation (AGE, Wallenberg Fellow), the Swedish Research Council VR (AGE, JH, JSF), and the USA National Institutes of Health (AGE). The authors thank Dr. Titti Ekegren and Prof Håkan Askmark at the Dept. of Neurology at Uppsala University for providing the samples.

ABBREVIATIONS

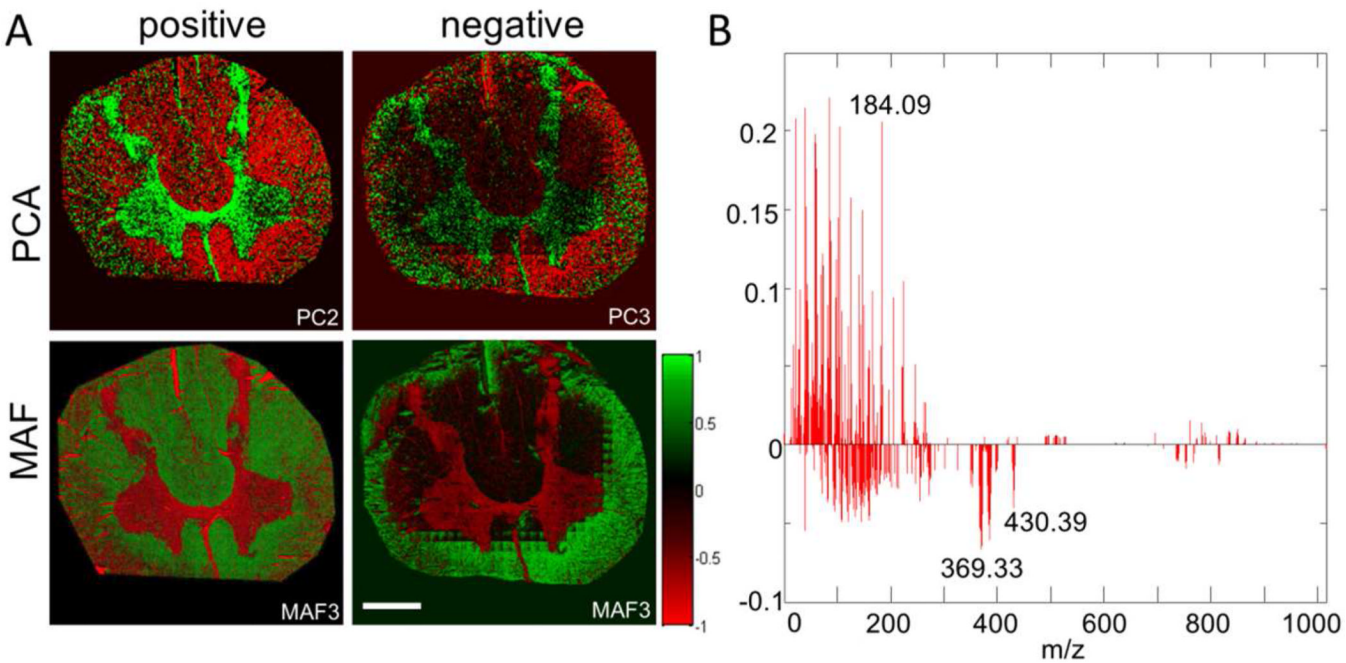
IMS	imaging mass spectrometry
ToF SIMS	time of flight secondary ion mass spectrometry
MALDI	matrix assisted laser desorption/ ionization
MVA	Multivariate statistical analysis
MAF	maximum autocorrelation factor
PCA	principal component analysis
SAM	statistical analysis of microarray data
ROI	region of interest
GM	grey matter
WM	white matter
VH	ventral horn
DH	dorsal horn
LH	lateral horn
DFL	dorsolateral fasciculus
SGR	substantia gelatinosa Rolando
PC	phosphatidylcholine
PI	phosphoinositol
FA	fatty acid

SM sphingomyeline

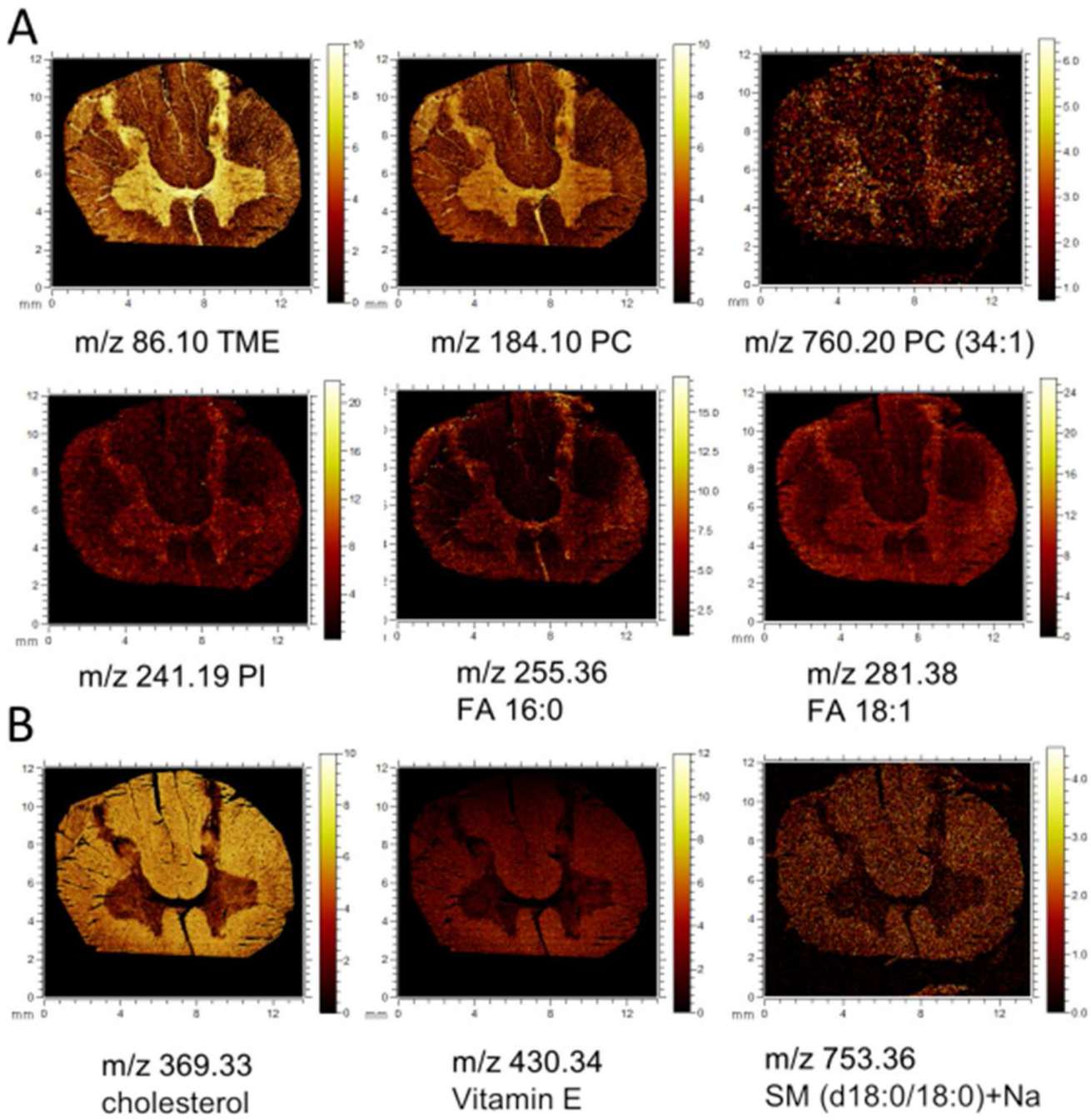
REFERENCES

1. Chio A. *Amyotroph Lateral Scler*. 2000; 1:S13–S18.
2. Cornett DS, Reyzer ML, Chaurand P, Caprioli RM. *Nat Methods*. 2007; 4:828–833. [PubMed: 17901873]
3. Benabdellah F, Seyer A, Quinton L, Touboul D, Brunelle A, Laprevote O. *Anal Bioanal Chem*. 2010; 396:151–162. [PubMed: 19711060]
4. Hanrieder J, Phan NTN, Kurczy ME, Ewing AG. *ACS Chem Neurosci*. 2013; 4:666–679. [PubMed: 23530951]
5. Nilsson A, Fehniger TE, Gustavsson L, Andersson M, Kenne K, Marko-Varga G, Andren PE. *PLoS ONE*. 2010; 5
6. Shariatgorji M, Nilsson A, Goodwin RJA, Svenningsson P, Schintu N, Banka Z, Kladni L, Hasko T, Szabo A, Andren PE. *Anal Chem*. 2012; 84:7152–7157. [PubMed: 22860714]
7. Spengler B, Hubert M. *J Am Soc Mass Spectrom*. 2002; 13:735–748. [PubMed: 12056573]
8. Jurchen JC, Rubakhin SS, Sweedler JV. *J Am Soc Mass Spectrom*. 2005; 16:1654–1659. [PubMed: 16095912]
9. Zavalin A, Todd EM, Rawhouser PD, Yang J, Norris JL, Caprioli RM. *J Mass Spectrom*. 2012; 47:1473–1481. [PubMed: 23147824]
10. Kollmer F. *Appl Surf Sci*. 2004; 231:153–158.
11. Touboul D, Kollmer F, Niehuis E, Brunelle A, Laprevote O. *J Am Soc Mass Spectrom*. 2005; 16:1608–1618. [PubMed: 16112869]
12. Weibel D, Wong S, Lockyer N, Blenkinsopp P, Hill R, Vickerman JC. *Anal Chem*. 2003; 75:1754–1764. [PubMed: 12705613]
13. Fletcher JS. *Analyst*. 2009; 134:2204–2215. [PubMed: 19838405]
14. Lazar AN, Bich C, Panchal M, Desbenoit N, Petit VW, Touboul D, Dauphinot L, Marquer C, Laprevote O, Brunelle A, Duyckaerts C. *Acta Neuropathol*. 2013; 125:133–144. [PubMed: 22956244]
15. Monroe EB, Annangudi SR, Hatcher NG, Gutstein HB, Rubakhin SS, Sweedler JV. *Proteomics*. 2008; 8:3746–3754. [PubMed: 18712768]
16. Van de Plas, R.; Ojeda, F.; Dewil, M.; Van Den Bosch, L.; De Moor, B.; Waelkens, E. *Pac Symp Biocomput*; 2007. p. 458–469.
17. Becker JS, Kumtabtim U, Wu B, Steinacker P, Otto M, Matusch A. *Metalomics*. 2012; 4:284–288. [PubMed: 22286961]
18. Girod M, Shi Y, Cheng J-X, Cooks RG. *Anal Chem*. 2011; 83:207–215. [PubMed: 21142140]
19. Girod M, Shi Y, Cheng JX, Cooks RG. *J Am Soc Mass Spectrom*. 2010; 21:1177–1189. [PubMed: 20427200]
20. Tucker KR, Lanni EJ, Serebryannyy LA, Rubakhin SS, Sweedler JV. *Anal Chem*. 2011; 83:9181–9185. [PubMed: 22017527]
21. Tucker KR, Serebryannyy LA, Zimmerman TA, Rubakhin SS, Sweedler JV. *Chem Sci*. 2011; 2:785–795. [PubMed: 21625333]
22. Crecelius AC, Cornett DS, Caprioli RM, Williams B, Dawant BM, Bodenheimer B. *J Am Soc Mass Spectrom*. 2005; 16:1093–1099. [PubMed: 15923124]
23. Tusher VG, Tibshirani R, Chu G. *Proc Natl Acad Sci USA*. 2001; 98:5116–5121. [PubMed: 11309499]
24. Henderson A, Fletcher JS, Vickerman JC. *Surf Interface Anal*. 2009; 41:666–674.
25. Tyler BJ, Rayal G, Castner DG. *Biomaterials*. 2007; 28:2412–2423. [PubMed: 17335898]
26. Hanrieder J, Wicher G, Bergquist J, Andersson M, Fex-Svenningsen A. *Anal Bioanal Chem*. 2011; 401:135–147. [PubMed: 21553124]
27. Passarelli MK, Winograd N. *Biochim Biophys Acta*. 2011; 1811:976–990. [PubMed: 21664291]

28. Sole-Domenech S, Sjovall P, Vukojevic V, Fernando R, Codita A, Salve S, Bogdanovic N, Mohammed AH, Hammarstrom P, Nilsson KP, LaFerla FM, Jacob S, Berggren PO, Gimenez-Llort L, Schalling M, Terenius L, Johansson B. *Acta Neuropathol.* 2013; 125:145–157. [PubMed: 22996963]
29. Sjovall P, Lausmaa J, Johansson B. *Anal Chem.* 2004; 76:4271–4278. [PubMed: 15283560]
30. Piwowar AM, Lockyer NP, Vickerman JC. *Anal Chem.* 2009; 81:1040–1048. [PubMed: 19125566]
31. Torres GE, Gainetdinov RR, Caron MG. *Nat Rev Neurosci.* 2003; 4:13–25. [PubMed: 12511858]
32. Bigdeli N, de Peppo GM, Lenneras M, Sjovall P, Lindahl A, Hyllner J, Karlsson C. *Tissue Eng Part A.* 2010; 16:3427–3440. [PubMed: 20653416]
33. Perrin FE, Gerber YN, Teigell M, Lonjon N, Boniface G, Bauchet L, Rodriguez JJ, Hugnot JP, Privat AM. *Cell Death Dis.* 2011; 2:e218. [PubMed: 21993394]
34. Sevigny CP, Bassi J, Williams DA, Anderson CR, Thomas WG, Allen AM. *J Comp Neurol.* 2012; 520:2352–2368. [PubMed: 22237784]
35. Rajaoefetra N, Passagia JG, Marlier L, Poulat P, Pellas F, Sandillon F, Verschuere B, Gouy D, Geffard M, Privat A. *J Comp Neurol.* 1992; 318:1–17. [PubMed: 1374763]
36. Kim KK, Adelstein RS, Kawamoto S. *J Biol Chem.* 2009; 284:31052–31061. [PubMed: 19713214]
37. Lund D, Ruggiero AM, Ferguson SM, Wright J, English BA, Reisz PA, Whitaker SM, Peltier AC, Blakely RD. *Neuroscience.* 2010; 171:1041–1053. [PubMed: 20888396]

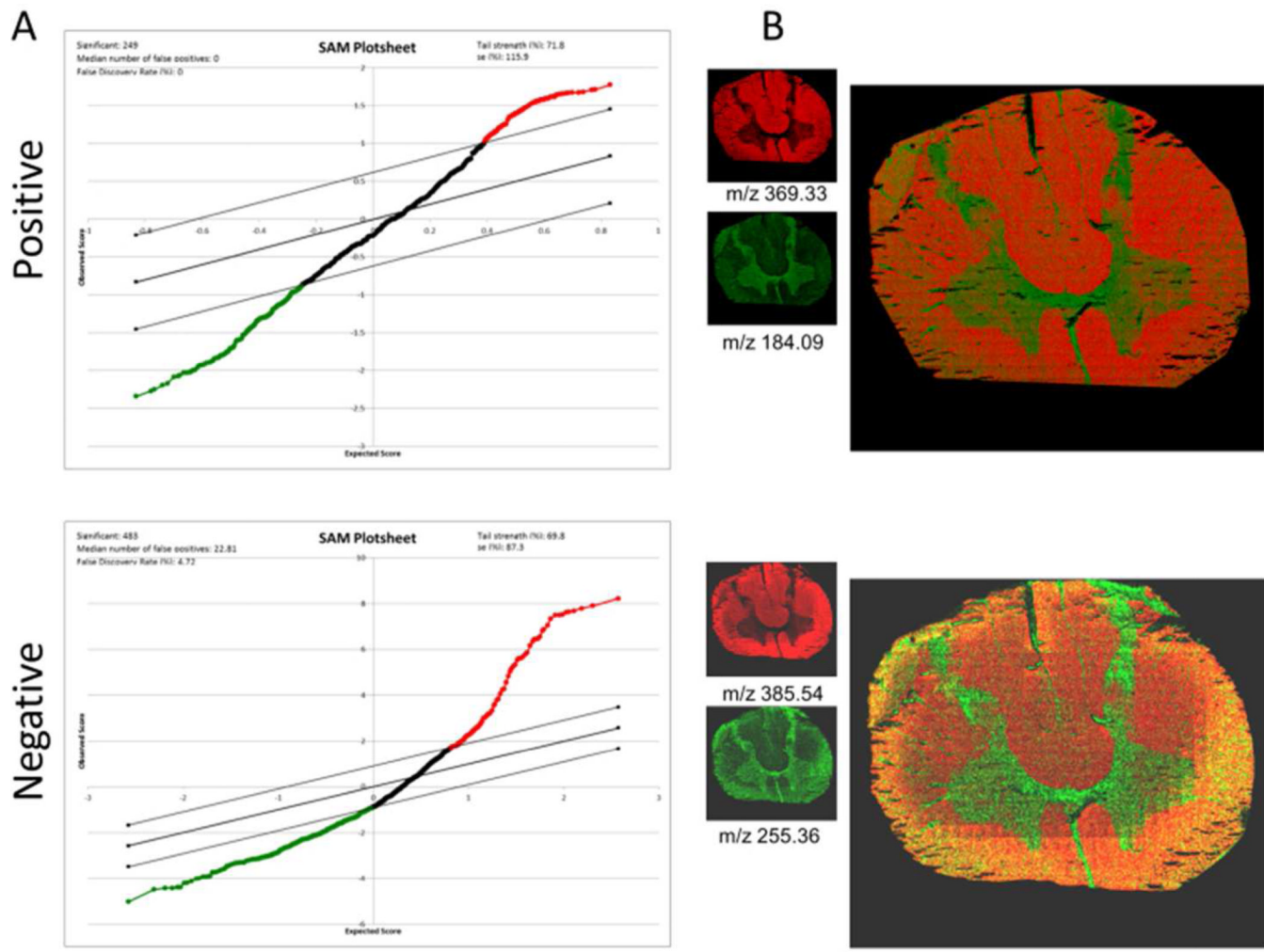
**Figure 1.**

Multivariate statistical analysis of imaging MS data by means of PCA and MAF reveals anatomical regions of human spinal cord including grey and white matter. **(A)** Composition images of corresponding MVA factors (i.e. principal components and MAF-factor) that allow identification of anatomical regions of interest. Each pixel intensity represents the respective score (eigenvalue). **(B)** The most influential variables (m/z values) for the respective factor can be deduced from the corresponding loadings. The figure illustrates the loadings of each m/z value in the PC2 (positive mode) for PCA image analysis. Detected masses corresponding to cholesterol (m/z 369.33, $C_{27}H_{45} [M+H-H_2O]^+$) and vitamin E (m/z 430.39, $C_{29}H_{50}O_2, [M+H]^+$) were found to be decreased, corresponding to negative intensity in the PCA image and were found to localize to the white matter. In contrast, masses corresponding to PC (m/z 184.09) were found to localize to grey matter. Scale bar = 5 mm. Please see SI Figure 6 for different color coding scheme.

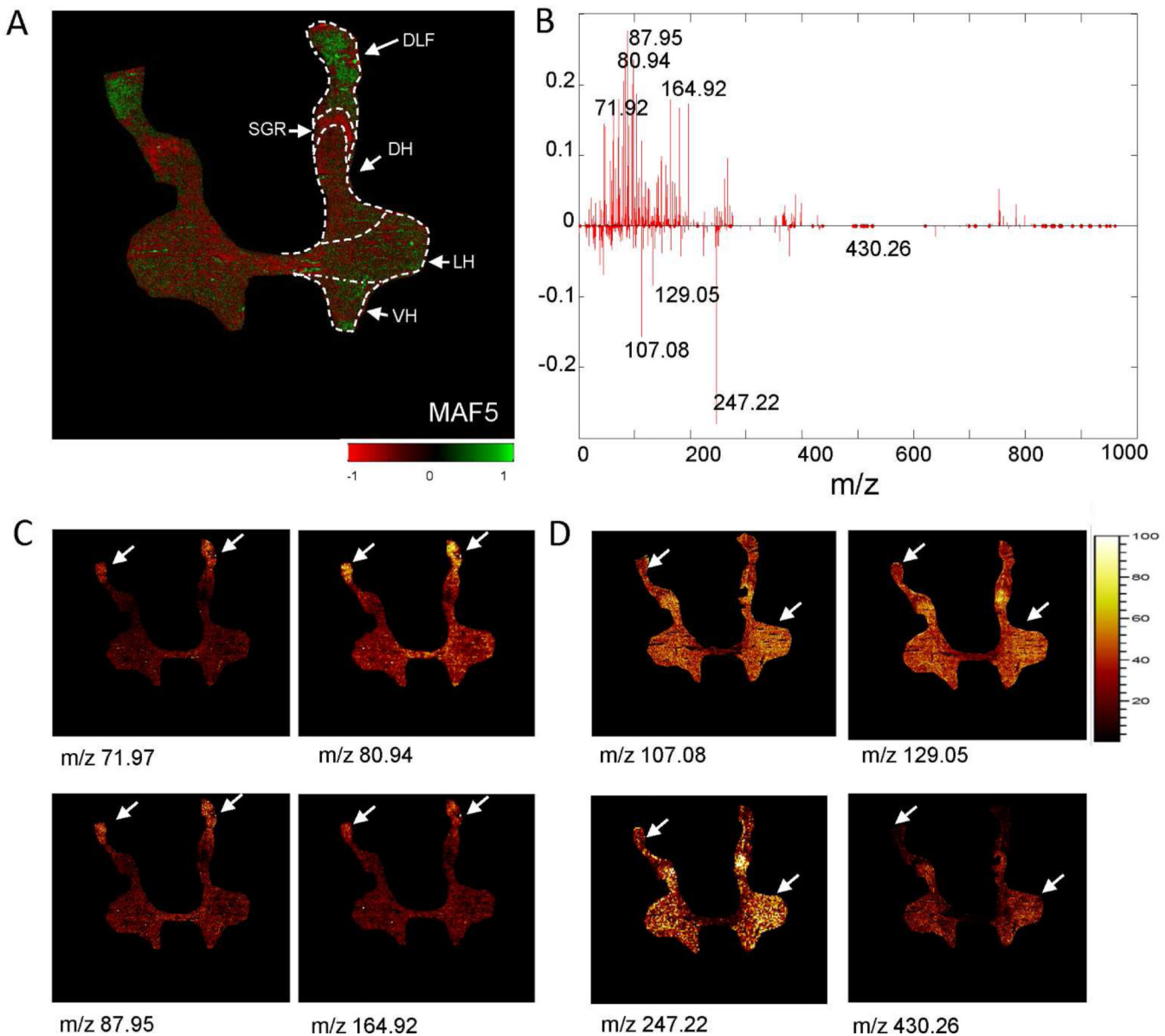
**Figure 2.**

Single ion images of individual molecular species that localize to distinct anatomical regions as revealed by multivariate images analysis. (A) Lipid species that localize to the grey matter including trimethylethylenimine (m/z 86.1, $[C_5H_{12}N]^+$), phosphatidylcholine headgroup ($[C_5H_{15}PO_4N]^+$, m/z 184.09), phospholipids in positive mode. In negative mode, phosphoinositol lipids (PI) as indicated by the PI headgroup (m/z 241.19, $[C_6H_{11}O_8P]^-$) as well as fatty acids (FA) such as palmitic acid (FA 16:0, m/z 255.36, $[C_{16}H_{31}O_2]^-$) and oleic acid (FA 18:1, m/z 281.38, $[C_{18}H_{33}O_2]^-$) were found increased in the grey matter. (B) Chemical species that localize to the white matter include cholesterol (m/z 369.33, $[M+H]$ -

$\text{H}_2\text{O}]^+$), vitamin E ($\text{C}_{29}\ \text{H}_{50}\text{O}_2$, $[\text{M}+\text{H}]^+$), and sphingolipids such as sphingomyelin (m/z 753.36, SM(d18:0/180) $[\text{M}+\text{Na}]^+$).

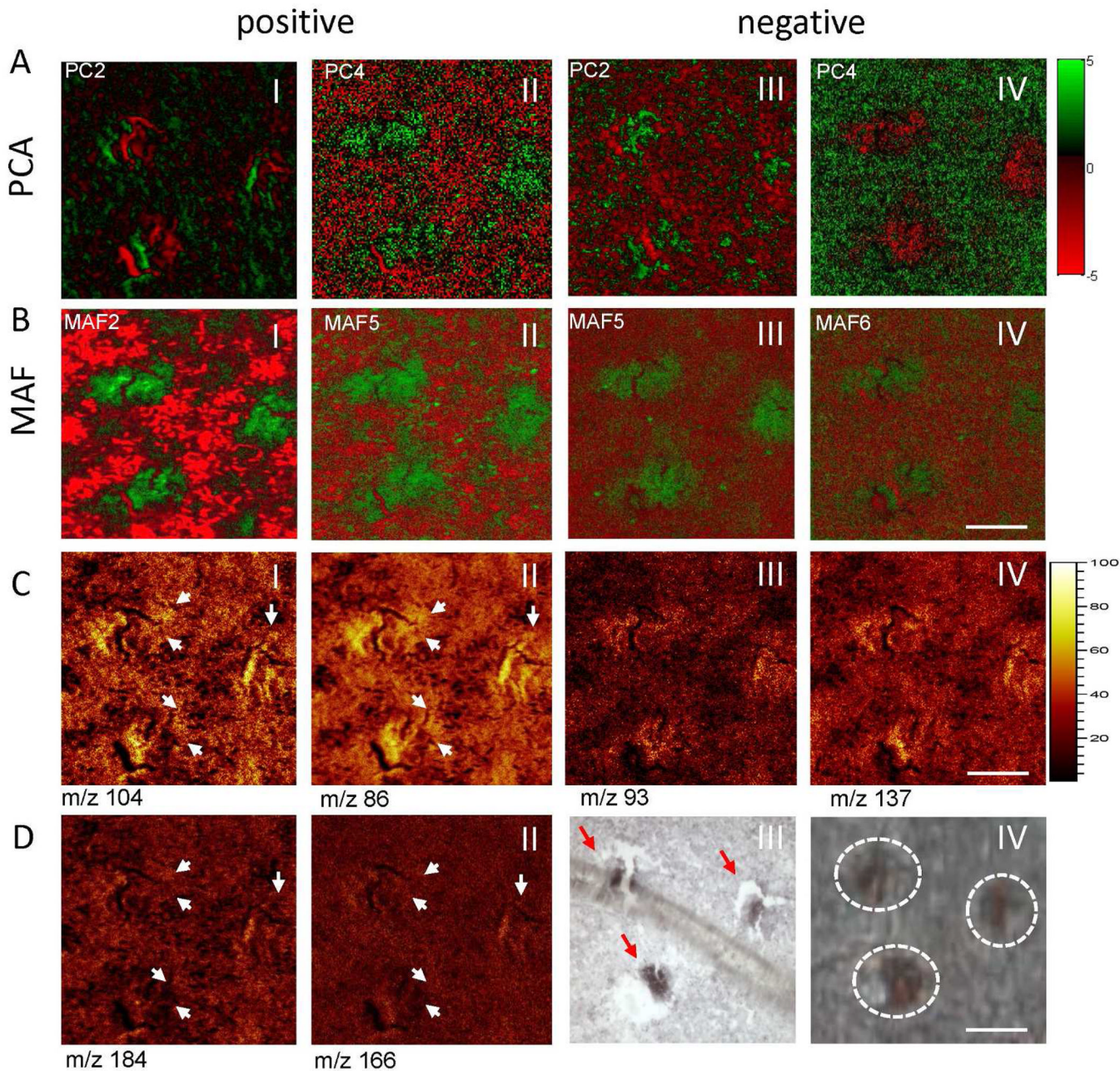
**Figure 3.**

Bottom up multivariate statistics in whole tissue section validates top-down findings. (A) MS data from previously outlined anatomical regions (grey and white matter) were subjected to multivariate, paired statistical analysis using an approach for statistical analysis of microarrays (SAM). The plot depicts the significance for a changed species (x-axis) and the degree of change (y-axis). Every single dot represents one compound (m/z value). Red color-coding indicates compounds that are relatively increased in the white matter such as cholesterol (m/z 369.33 $[M+H-H_2O]^+$, m/z 385.54 $[M-H]^+$) similarly to PCA and MAF results. Green color-coding indicates compounds to be relatively decreased in the white matter compared to the grey matter such as PC (m/z 184.09, $[M+H]^+$) and palmitic acid (FA 16:0, m/z 255.36, $[C_{16}H_{31}O_2]^-$) as verified by single ion images and overlay images that confirm distinct localization of these compounds to the respective anatomical region (B). Please see SI Figure 7 for different color coding scheme.

**Figure 4.**

Multivariate image analysis reveals intra-ROI heterogeneity. MAF- but not PCA-based image analysis reveal chemical differences in the grey matter. (A) Molecular species are characteristically changed in anatomical sub-regions of the spinal cord, including the dorsolateral fasciculus (DFL), the substantia gelatinosa Rolando (SGR), the lateral horn (LH), the dorsal horn (DH) and the ventral horn as demonstrated in the composition image. Here the color coding indicates the magnitude of respective MAF scores for each pixel (spectrum) over the whole tissue section and thereby reveal chemical differences. These differences can be deduced from the loading data of the corresponding MAF-factor (B). The spectrum shows which compounds (m/z) change over the whole grey matter region. The most intense changes can relate to spatial changes in between the sub regions. (C) Single ion images of compounds that were found increased in the dorsolateral fasciculus as revealed by MAF and verified by bottom up analysis with SAM. (D) Similarly, MVA reveals

compounds relatively increased in the SGR (arrow) or ventral or intermediate part of the grey matter. Please see SI Figure 8 for different color coding scheme.

**Figure 5.**

Subcellular imaging of single motor neurons. (A,B) Multivariate statistical analysis (MVA) of imaging data acquired in burst align (BA) mode at submicron resolution using PCA (A) and MAF (B). Data were acquired in both positive (A I-II, B I-II) and negative ion mode (A III-IV, B III-IV) and analyzed. The respective MVA factors show detection of cell-like features, where MAF demonstrated better contrast. Analysis of MVA loading data and verification with single ion images demonstrated a better performance for MAF compared to PCA, as verified by true localizations of MVA deduced loading values. (C) In positive mode MAF (MAF-factor 2), revealed a neuron-specific localization of choline (m/z 104, C-I) and its fragment trimethylethenamine (m/z 86, C-II). Similarly, yet unknown compounds at m/z 93 (C-III) and 137 (C-IV) were found to localize to the cells as revealed by MAF (MA-

factor 5). (D) Single ion images of phosphatidylcholine headgroup (m/z 184, D-I) and its fragment (m/z 166, D-II) showed no distinct localization to the cell bodies (arrows). Immunohistochemical staining against neuronal marker NeuN (D-III) verified the neuronal identity microscopic detected cell features (arrows) depicted in D-IV. Scale bar = $30\mu\text{m}$. Please see SI Figure 9 for different color coding scheme.